



Claudins are essential for cell shape changes and convergent extension movements during neural tube closure

Amanda I. Baumholtz^{a,e}, Annie Simard^{b,e}, Evanthia Nikolopoulou^f, Marcus Oosenbrug^{c,e}, Michelle M. Collins^{a,e,1}, Anna Piontek^g, Gerd Krause^g, Jörg Piontek^h, Nicholas D.E. Greene^f, Aimee K. Ryan^{a,b,d,e,*}

^a Department of Human Genetics, McGill University, Canada

^b Department of Experimental Medicine, McGill University, Canada

^c Department of Anatomy and Cell Biology, McGill University, Canada

^d Department of Pediatrics, McGill University, Canada

^e The Research Institute of the McGill University Health Centre, Montréal, Québec, Canada

^f Developmental Biology and Cancer Programme, Birth Defects Research Centre, UCL Institute of Child Health, London, UK

^g Leibniz-Forschungsinstitut für Molekulare Pharmakologie, FMP, Berlin, Germany

^h Institute of Clinical Physiology, Charité-Universitätsmedizin Berlin, Berlin, Germany

ARTICLE INFO

Keywords:

Claudin
Neural tube defects
Tight junctions
Apical constriction
Convergent extension

ABSTRACT

During neural tube closure, regulated changes at the level of individual cells are translated into large-scale morphogenetic movements to facilitate conversion of the flat neural plate into a closed tube. Throughout this process, the integrity of the neural epithelium is maintained via cell interactions through intercellular junctions, including apical tight junctions. Members of the claudin family of tight junction proteins regulate paracellular permeability, apical-basal cell polarity and link the tight junction to the actin cytoskeleton. Here, we show that claudins are essential for neural tube closure: the simultaneous removal of Cldn3, -4 and -8 from tight junctions caused folate-resistant open neural tube defects. Their removal did not affect cell type differentiation, neural ectoderm patterning nor overall apical-basal polarity. However, apical accumulation of Vangl2, RhoA, and pMLC were reduced, and Par3 and Cdc42 were mislocalized at the apical cell surface. Our data showed that claudins act upstream of planar cell polarity and RhoA/ROCK signaling to regulate cell intercalation and actin-myosin contraction, which are required for convergent extension and apical constriction during neural tube closure, respectively.

1. Introduction

The molecular interactions that regulate many of the morphogenetic changes required for neural tube closure occur at the apical cell surface (Colas and Schoenwolf, 2001; Lawson et al., 2001). Apical localization of Wnt/planar cell polarity (PCP) pathway components is required for the convergent extension movements that lead to anterior-posterior elongation and medial-lateral narrowing of the neural plate (Goto and Keller, 2002; Wallingford and Harland, 2002; Wang et al., 2006). Apical constriction of cells at the midline to form the median hinge point depends upon the actin-myosin contractile force driven by localized myosin light chain phosphorylation

downstream of RhoA-ROCK signaling (Suzuki et al., 2012; Kinoshita et al., 2008). This allows the neural plate to bend and the neural folds to elevate. During the final phase of neural tube closure, Cdc42 RhoGTPase signaling regulates the formation of apical protrusions which are essential for the epithelial remodeling at the boundary of the neural and non-neural ectoderm to form the closed neural tube and a continuous layer of overlying surface ectoderm (Lawson et al., 2001; Pai et al., 2012; Moury and Schoenwolf, 1995).

Apical tight junctions are a hallmark of vertebrate epithelial cell layers. They maintain apical-basal polarity by preventing the mixing of apical and basolateral membrane proteins and regulate the paracellular movement of ions, solutes and water (Gunzel and Yu, 2013; Suzuki et al., 2015). The

Abbreviations: C-CPE, C-terminal domain of *Clostridium perfringens* enterotoxin; NTD, Neural tube defect

* Correspondence to: Centre for Translational Biology, RI-MUHC, Room EM0.3211, 1001 Décarie Boulevard, Montréal, Québec, Canada H4A 3J1.

E-mail addresses: amanda.baumholtz@mail.mcgill.ca (A.I. Baumholtz), annie.simard2@mail.mcgill.ca (A. Simard), e.nikolopoulou@ucl.ac.uk (E. Nikolopoulou), marcus.oosenbrug@mail.mcgill.ca (M. Oosenbrug), michelle.collins@mpi-bn.mpg.de (M.M. Collins), apiontek@fmp-berlin.de (A. Piontek), gkrause@fmp-berlin.de (G. Krause), joerg.piontek@charite.de (J. Piontek), n.greene@ucl.ac.uk (N.D.E. Greene), aimee.ryan@mcgill.ca (A.K. Ryan).

¹ Present Address: Max Planck Institute for Heart and Lung Research, Bad Nauheim, Germany.

<http://dx.doi.org/10.1016/j.ydbio.2017.05.013>

Received 14 March 2017; Received in revised form 8 May 2017; Accepted 14 May 2017

Available online 22 May 2017

0012-1606/© 2017 The Authors. Published by Elsevier Inc. This is an open access article under the CC BY license (<http://creativecommons.org/licenses/by/4.0/>).

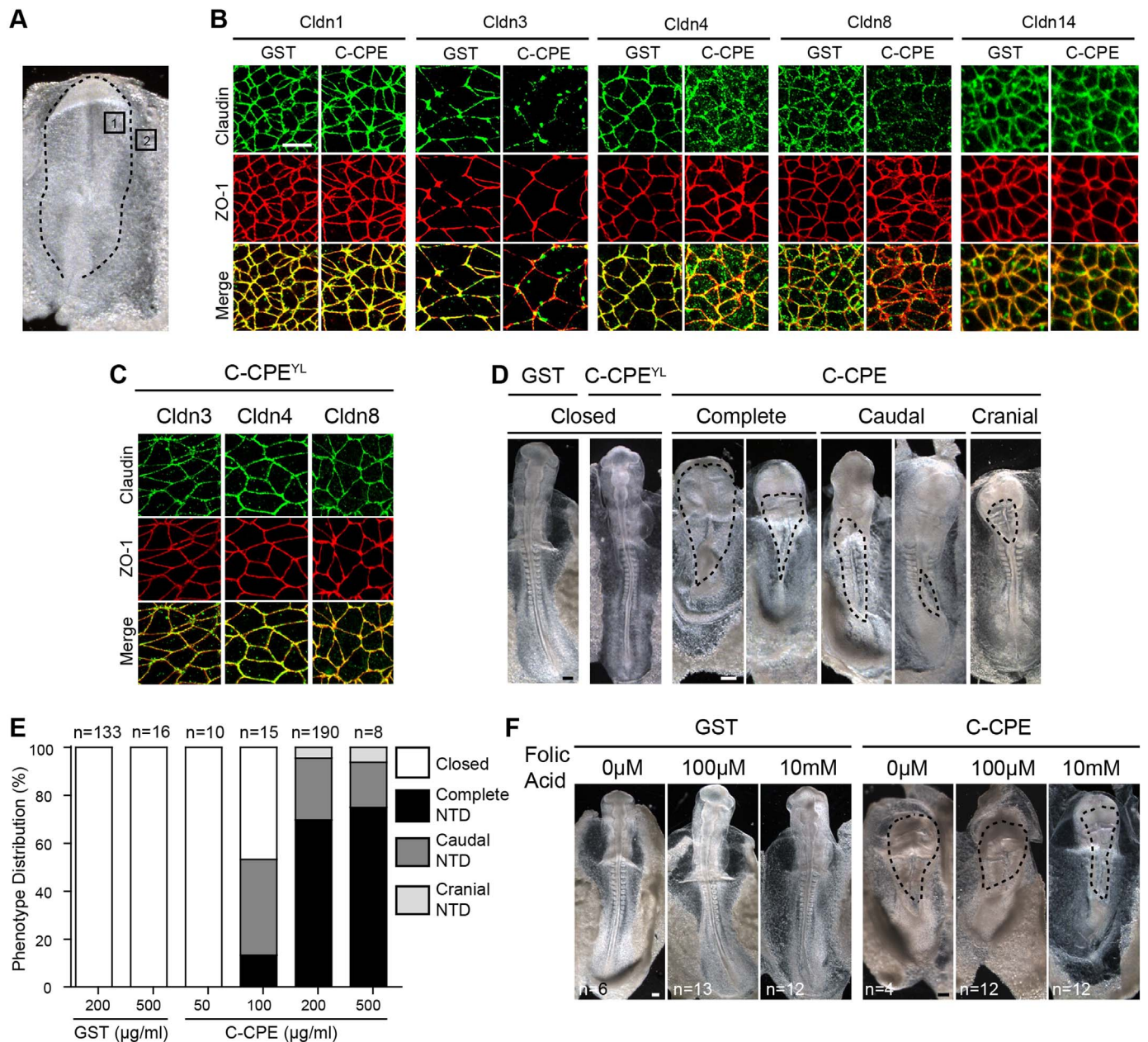


Fig. 1. C-PE-treated embryos exhibit dose-dependent, folic acid resistant neural tube defects. **(A)** Dorsal view of a neural groove stage embryo. Dashed line outlines the neural plate. The areas of the neural (box 1) and non-neural (box 2) ectoderm imaged in **(B)** are shown. **(B)** Apical surface view of ZO-1 (red) and Cldn1, -4, -8 or -14 (green) in the neural ectoderm and Cldn-3 (green) in non-neural ectoderm of 5 h GST- or C-PE-treated embryos. Three embryos per treatment were analyzed. Scale bar, 10 μm. **(C)** Apical surface views of ZO-1 (red) and Cldn3, -4 or -8 (green) in embryos treated with C-PE^{YL} for 5 h. Three embryos per treatment were analyzed. Scale bar, 10 μm. **(D)** Dorsal views of chick embryos treated with 200 μg/ml GST, C-PE^{YL}, or C-PE for 20 h. Dashed lines indicate open neural tubes. Scale bar, 0.2 mm. **(E)** Distribution of complete, cranial and caudal open NTDs following 20 h incubation in 200 or 500 μg/ml GST or 50, 100, 200 or 500 μg/ml C-PE. **(F)** Dorsal views of embryos treated with 200 μg/ml GST or C-PE in the presence of 0 μM, 100 μM, or 1 mM folic acid. Dashed lines indicate open neural tubes. Scale bar, 0.2 mm.

claudin family of tetraspan membrane proteins are essential for formation of the tight junction backbone through homo- and heteropolymerization: their four transmembrane helix bundles interact within one cell membrane and their two extracellular loops interact with those of claudins in the apposing cell (Gunzel and Yu, 2013; Daugherty et al., 2007 Krause et al., 2015). While the claudin extracellular loops define the paracellular barrier properties of the junction, their cytoplasmic C-termini interact with adaptor and scaffolding protein complexes at the tight junction cytoplasmic plaque. Thus, claudins are poised at the apical surface to bridge intercellular interactions to cytoplasmic regulatory events that affect cell behaviours.

Our previous analysis of claudin expression patterns in chick embryos revealed that 14 claudins are expressed during neurulation

(Collins et al., 2013). Neural tube defects have not been reported in any of the single claudin knockout mouse lines (Anderson et al., 2006 Ben-Yosef et al., 2003; Fujita et al., 2012; Furuse et al., 2002; Gow et al., 1999; Kage et al., 2014; Li et al., 2014; Miyamoto et al., 2005; Morita et al., 1999; Tamura et al., 2006;). However, *Cldn4*, -6, and -7 are downregulated in *Grhl2* mutant mouse lines, which exhibit open neural tube defects due to a failure in the final stage of neural tube closure (Rifat et al., 2010; Pyrgaki et al., 2011; Werth et al., 2010). These data suggest that claudins may have functionally redundant roles during neural tube closure.

The C-terminal domain of *C. perfringens* enterotoxin (C-PE) is an ideal tool for studying claudin redundancy. Full-length CPE, a common cause of food poisoning, crosses the intestinal barrier at tight junctions



Movie 1. The heart of C-CPE-treated embryos is beating. Movie showing the beating heart of a C-CPE-treated embryo (left) cultured *ex ovo* using the Cornish Pasty method for 20 h. **Movie 1 Still.** Ventral view showing the rightwardly looped heart tube of a C-CPE-treated embryo. Supplementary material related to this article can be found online at <http://dx.doi.org/10.1016/j.ydbio.2017.05.013>.

by binding to the second extracellular loop of Cldn4, which was first cloned as the CPE cell-surface receptor (CPE-R) (Katahira et al., 1997a). CPE also interacts with Cldn3, -6, -7, -8, -9, -14 and -19 (Katahira et al., 1997b; Winkler et al., 2009; Shrestha and McClane, 2013) but not with other cell surface proteins (Katahira et al., 1997b; Lohrberg et al., 2009). C-CPE contains the claudin binding domain but not the cytotoxic domain, which is located in the N-terminal region of CPE. C-CPE can bind to and internalize the same subset of claudins without affecting the localization of other claudin family members (Winkler et al., 2009; Sonoda et al., 1999). C-CPE was used to demonstrate the redundant functions of Cldn4 and -6 in mouse blastocysts: mice null for only Cldn4 (Fujita et al., 2012) or only Cldn6 (Anderson et al., 2006) are viable but removal of both claudins by C-CPE caused a loss of the hydrostatic pressure that maintains blastocoel shape (Moriwaki et al., 2007).

Here, we determined that C-CPE-sensitive claudins are essential for neural tube morphogenesis. Targeted removal of Cldn3, -4 and -8 from the neural and non-neural ectoderm of neural plate stage chick embryos resulted in folate-resistant open neural tube defects (NTDs). We showed that C-CPE-sensitive claudins were required for convergent extension movements and apical constriction of cells at the median hinge point. Furthermore, our data suggest that claudin family members differentially regulate localization of components of the PCP polarity complex and RhoGTPase signaling to the apical cell surface.

2. Results

2.1. C-CPE-sensitive claudins are required for neural tube closure in chick embryos

To simultaneously remove multiple claudins from tight junctions during neurulation we used the nontoxic GST-C-CPE (hereafter referred to as C-CPE) reagent and compared its effects to either GST alone or C-CPE^{YL}, a variant of C-CPE that does not bind claudins (Protze et al., 2015). Previously we showed by whole mount *in situ* hybridization that *Cldn3*, -4, -8 and -14 are the only C-CPE-sensitive claudins expressed during neural tube closure in chick embryos. We first confirmed that the protein expression patterns of these claudins during neural tube closure matched that of their transcripts (Collins et al., 2013). As expected Cldn4, -8 and -14 were expressed in the neural ectoderm, while Cldn3 was absent from the neural folds but was highly expressed in non-neural ectoderm (Supplementary Fig. 1). Next, we tested the ability of C-CPE to effectively remove these claudins from

tight junctions as compared to effects on Cldn1, which does not interact with C-CPE (Fig. 1A and B). In GST-treated embryos, all five claudins co-localized with the tight junction scaffolding protein ZO-1 at apical cell-cell contacts in the neural (Cldn1, -4, -8, -14) and non-neural (Cldn1, -3, -4, -14) ectoderm (Fig. 1B). Co-localization analysis using Pearson's correlation coefficient confirmed that Cldn1 (R=0.6267), -3 (R=0.5583), -4 (R=0.5867), -8 (R=0.5070), and -14 (R=0.7156) co-localized at tight junctions with ZO-1, which was used as a marker of tight junctions. After 5 h of C-CPE treatment, only Cldn1 (R=0.6975) and Cldn14 (R=0.6083) remained co-localized with ZO-1 at tight junctions; localization of Cldn3 (R=0.09563), -4 (R=0.09) and -8 (R=0.2519) was discontinuous and often absent (Fig. 1B). Similar effects were observed after 20 h (data not shown). The unexpected observation that Cldn14 remained localized to tight junctions in C-CPE-treated embryos may reflect context-dependent sensitivity to C-CPE. As predicted, C-CPE^{YL} had no effect on the localization of Cldn3, -4 or -8 (Fig. 1C).

To determine if C-CPE-sensitive claudins are required for neural tube closure, HH4 neural plate stage embryos were cultured *ex ovo* in GST or in C-CPE media for 20 h. GST-treated embryos and embryos treated with the C-CPE^{YL} variant were indistinguishable from wild type embryos grown *in ovo* (Fig. 1D). C-CPE-treatment did not affect embryo viability: at 20 h their hearts were beating, of normal size and exhibited normal rightward looping (Movie 1; Supplementary Fig. 2). However, C-CPE-treated embryos showed a dose-dependent increase in the incidence of open NTDs (Fig. 1E). NTDs were characterized as 'complete' when the opening was along the entire anterior-posterior axis, 'caudal' when the opening was posterior to the hindbrain or 'cranial' when the opening was in the region of the future brain (Fig. 1D and E). The lowest dose of C-CPE that caused NTDs in 100% of embryos (200 µg/ml) was used for all subsequent experiments. Folic acid supplementation, which reduces the incidence of NTDs in humans by 60–70% (van der Linden et al., 2006) and rescues NTDs induced in chick embryos (Guney et al., 2003; Weil et al., 2004), was unable to rescue the NTDs in C-CPE-treated embryos (n=24; Fig. 1F), suggesting that the C-CPE-induced NTDs are a model of folate-resistant NTDs.

2.2. Evolutionarily-conserved requirement for claudins in neural tube closure in mice

To determine if removal of C-CPE-sensitive claudins would affect neural tube closure in mouse embryos, C-CPE was injected into the amniotic cavity of embryos that were then cultured for approximately 18 h (Fig. 2A). Among embryos injected at the 0–4 somite stage, exposure to 0.5 or 1 mg/ml led to shortening of the caudal end of the embryo and a 'wiggly' neural tube suggestive of caudal elongation defects and a proportion of these embryos (n=4/7) also failed to undergo axial turning. As these embryos did not progress to a stage where neural tube closure could be reliably assessed due to other confounding phenotypes, we focused our analysis on embryos in which treatment was performed after initiation of neural tube closure at the 9–13 somite stage. Treated embryos appeared healthy and viable after the culture period; yolk sac circulation and mean number of somites in C-CPE-treated embryos did not significantly differ from controls. Spinal neural tube closure continued to progress in all treatment groups. However, the open region of spinal neural folds (posterior neuropore) was significantly larger in embryos treated with C-CPE (Fig. 2C,D) than in GST controls (Fig. 2B), indicating suppression of closure. Moreover, cranial NTDs were also observed in embryos exposed to 0.5 (n=1/8) and 1 mg/ml (n=3/12) C-CPE (Fig. 2D). These data indicate that C-CPE-sensitive claudins are also required for neural tube closure in mouse embryos. The 'milder' NTDs observed in the C-CPE-treated mouse embryos most likely reflects the fact that neural tube closure was already initiated at the time of treatment.

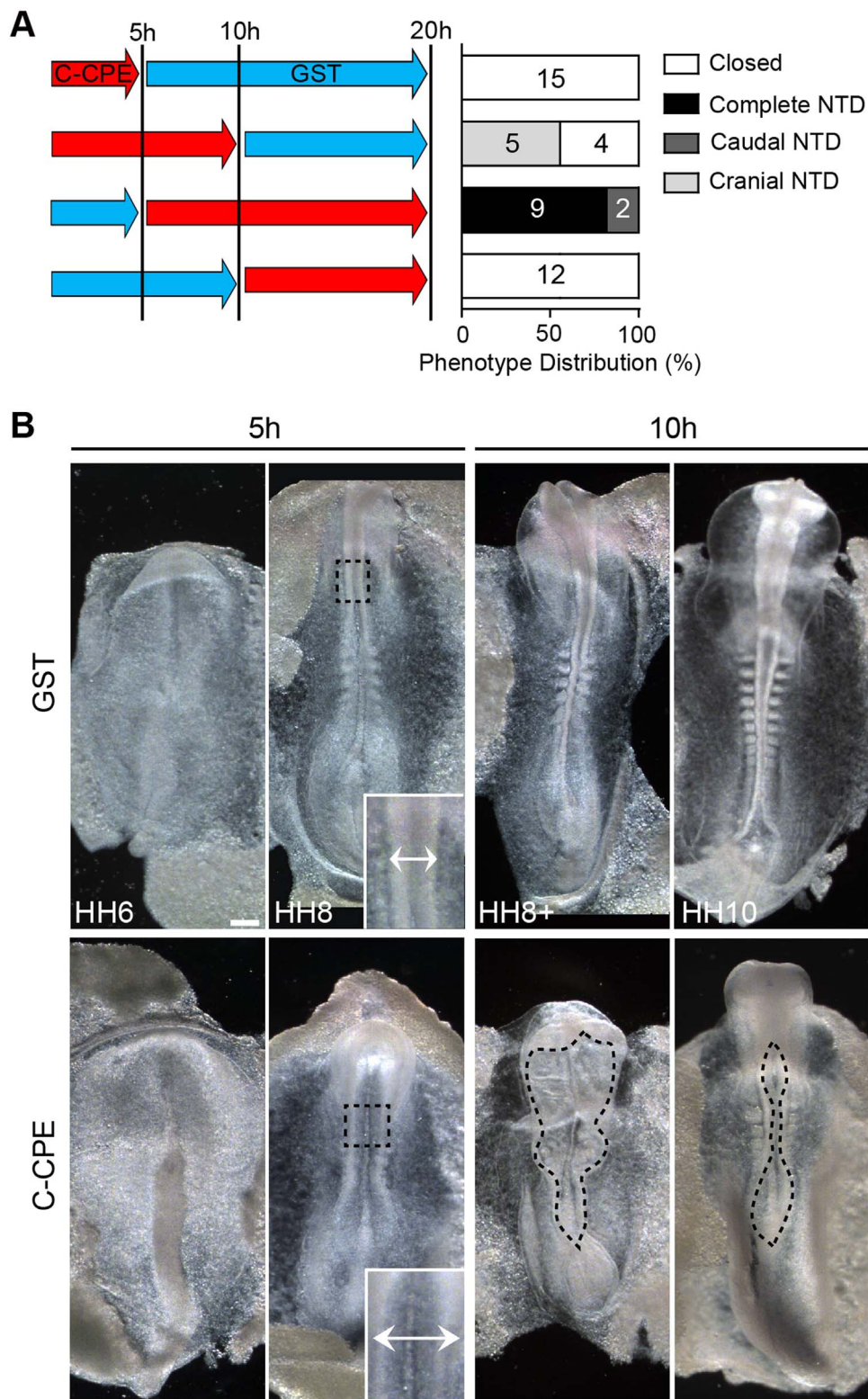


Fig. 3. C-CPE-sensitive claudins are required for apposition of neural folds. **(A)** Time course of media swap (left) and phenotypes of neural tube defects at the end of the 20 h of culture period (right). Numbers of embryos per phenotype are indicated. **(B)** Dorsal views of embryos cultured from the neural plate stage (HH4) in 200 µg/ml GST or C-CPE for 5 h or 10 h. Double-headed arrows indicate distance between midbrain neural folds (inset). Dashed lines outline open NTDs. Scale bar, 0.2 mm.

reduced length-to-width ratio ($p < 0.001$) at all stages of neurulation examined (Fig. 4A,B). Second, the somites of 20–40 h C-CPE-treated embryos were irregularly shaped and sometimes fused (Fig. 4C-F). Third, the notochord marker *Brachyury (T)* had a broadened posterior expression domain and the notochords were misshapen in 50% of the C-CPE-treated embryos (Fig. 4G). Finally, we observed an effect on

oriented cell division, which helps shape the neural plate (Sausedo et al., 1997). In GST-treated embryos, mitotic spindles in the neural ectoderm were preferentially oriented rostrocaudally ($p=0.031$), while in C-CPE-treated embryos there was a decrease in the proportion of rostrocaudal divisions and corresponding increase in mediolateral divisions ($p=0.125$) (Fig. 4H). Together these data suggest that removal

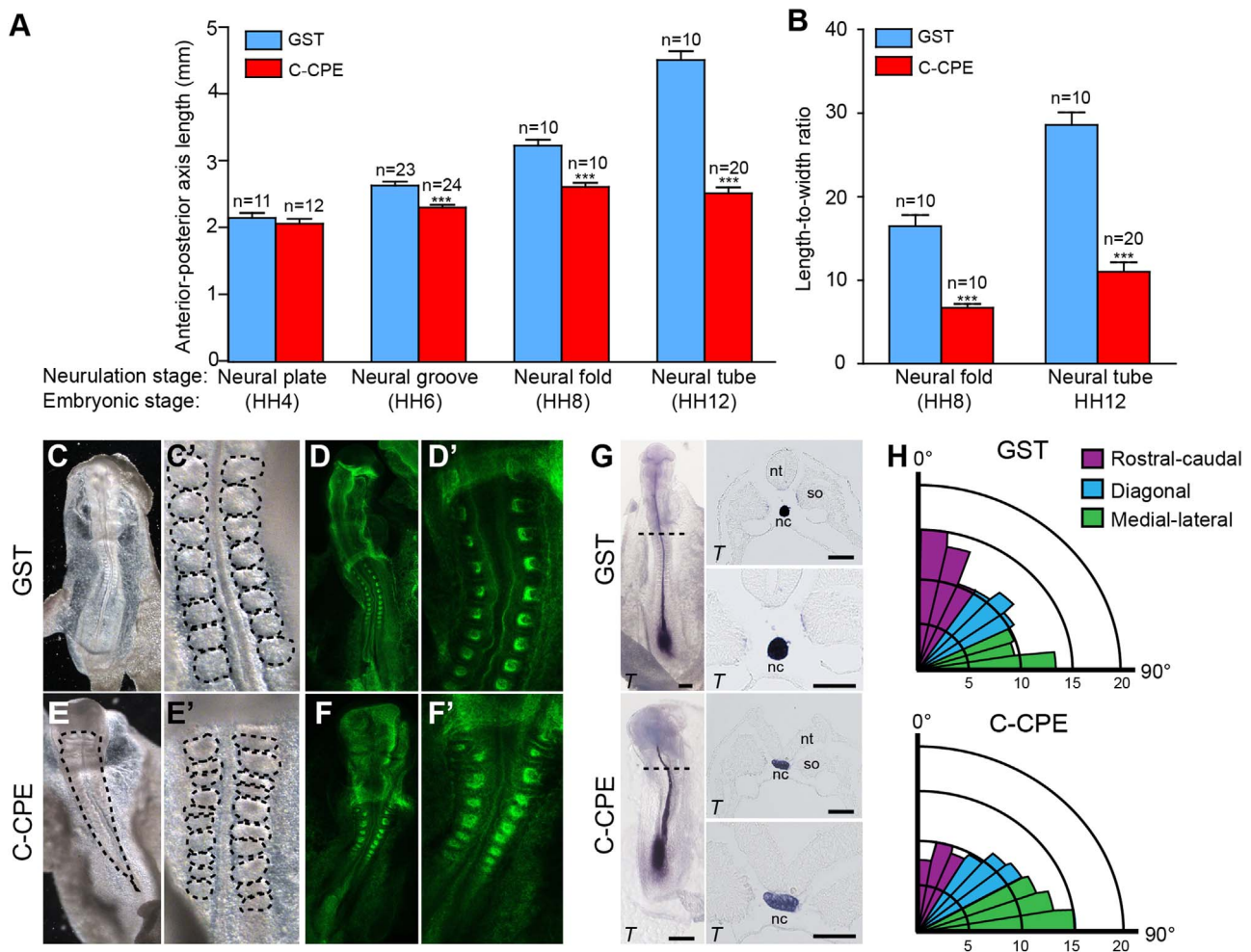


Fig. 4. C-PE-treated embryos exhibit convergent extension defects. **(A)** Graph shows average anterior-posterior (AP) length of GST- and C-PE-treated embryos at different stages of neural tube closure (mean \pm s.e.m., *** p < 0.0001, Mann-Whitney U -test). Corresponding Hamilton and Hamburger (HH) stages are indicated below. **(B)** Graph shows length-to-width ratio for GST- and C-PE-treated embryos at neural fold and neural tube stages (mean \pm s.e.m., *** p < 0.0001, Mann-Whitney U -test). **(C-F)** Dorsal views of embryos treated with 200 μ g/ml GST (C, D) or C-PE (E, F) for 20 h. Brightfield images (C, E) and Phalloidin-stained (D, F) embryos are shown. (C', D') Higher magnification images showing paired somites in GST-treated embryos (C', D') and unpaired and fused somites in C-PE-treated embryos (E', F'). **(G)** Left, dorsal view of *Brachyury* (*T*) expression following 20 h treatment with 200 μ g/ml GST or C-PE for 20 h. Scale bar, 0.5 mm. Right, transverse section corresponding to position indicated. Bottom images are higher magnification images of sections. Scale bar, 50 μ m. nc, notochord; nt, neural tube; so, somite. **(H)** Rose diagram showing orientation of cell divisions relative to the midline in GST- ($n=6$ embryos/810 cells) and C-PE-treated embryos ($n=4$ embryos/629 cells) at 5 h. Division angles are binned in bins of 10° from 0° to 90°. Purple bars represent rostrocaudal (RC) divisions, blue are mediolateral (ml) divisions, and green are diagonal (D) divisions. In GST-treated embryos, mitotic spindles are oriented preferentially in the RC plane compared to the ml plane ($p=0.031$) in C-PE-treated embryos cell division was random ($p=0.125$) (Wilcoxon's signed-ranks test).

of C-PE-sensitive claudins prevents normal convergent extension movements during neurulation, contributing to the increased distance between the neural folds thereby impeding neural fold fusion.

The broadened neural groove in C-PE-treated embryos suggested a failure in median hinge point formation. In GST-treated embryos, *Shh* exhibited a normal wedge-shaped expression domain at the neural plate midline reflecting the triangular shape of these cells (Fig. 5A). In C-PE-treated embryos *Shh* expression was unaffected but the shape of its expression domain was rectangular rather than the triangular shape observed in control embryos (Fig. 5A). Indeed, transmission electron microscopy confirmed that midline neural tube cells in C-PE-treated embryos were not apically constricted and triangular (Fig. 5B). The apical-to-basal width ratio of the midline cells was three times greater in C-PE-treated embryos than in GST-treated embryos ($p=0.012$; Fig. 5C). Microtubule-dependent basal migration of the nuclei also contributes to the basal widening of the median hinge point cells (Smith and Schoenwolf, 1987; Karfunkel, 1971; 1972). As expected, median hinge point cell nuclei were situated basally in GST-treated embryos (Fig. 5D). However, in C-PE-treated embryos, these nuclei were randomly localized and on average closer to the apical surface

than in GST-treated control embryos ($p=0.0005$) (Fig. 5D,E). In addition, the apical-basal microtubule network was discontinuous in C-PE-treated embryos (Fig. 5F). Together these data demonstrate that C-PE-sensitive claudins are required in the neural ectoderm for cell shape changes associated with median hinge point formation.

2.6. Claudins function upstream of PCP and RhoA/ROCK signaling

Convergent extension and apical constriction during neurulation require the coordinated activities of the PCP and RhoA/ROCK signaling pathways, respectively (Nishimura et al., 2012; Kinoshita et al., 2008; Ossipova et al., 2015). In order to position claudins in the context of these pathways, we examined the expression of Vangl2, a core component of the PCP pathway that is required for neural tube closure (Murdoch et al., 2001; Kibar et al., 2011), RhoA, a small GTPase that shuttles between the cytoplasm and membrane, and phosphorylated myosin light chain (pMLC), the downstream target of RhoA/ROCK signaling. Vangl2 was greatly reduced after 5 h of C-PE-treatment ($p=0.0024$) (Fig. 6A). RhoA partly co-localized with ZO-1 and Cldn14 at the membrane in the neural ectoderm of GST-treated

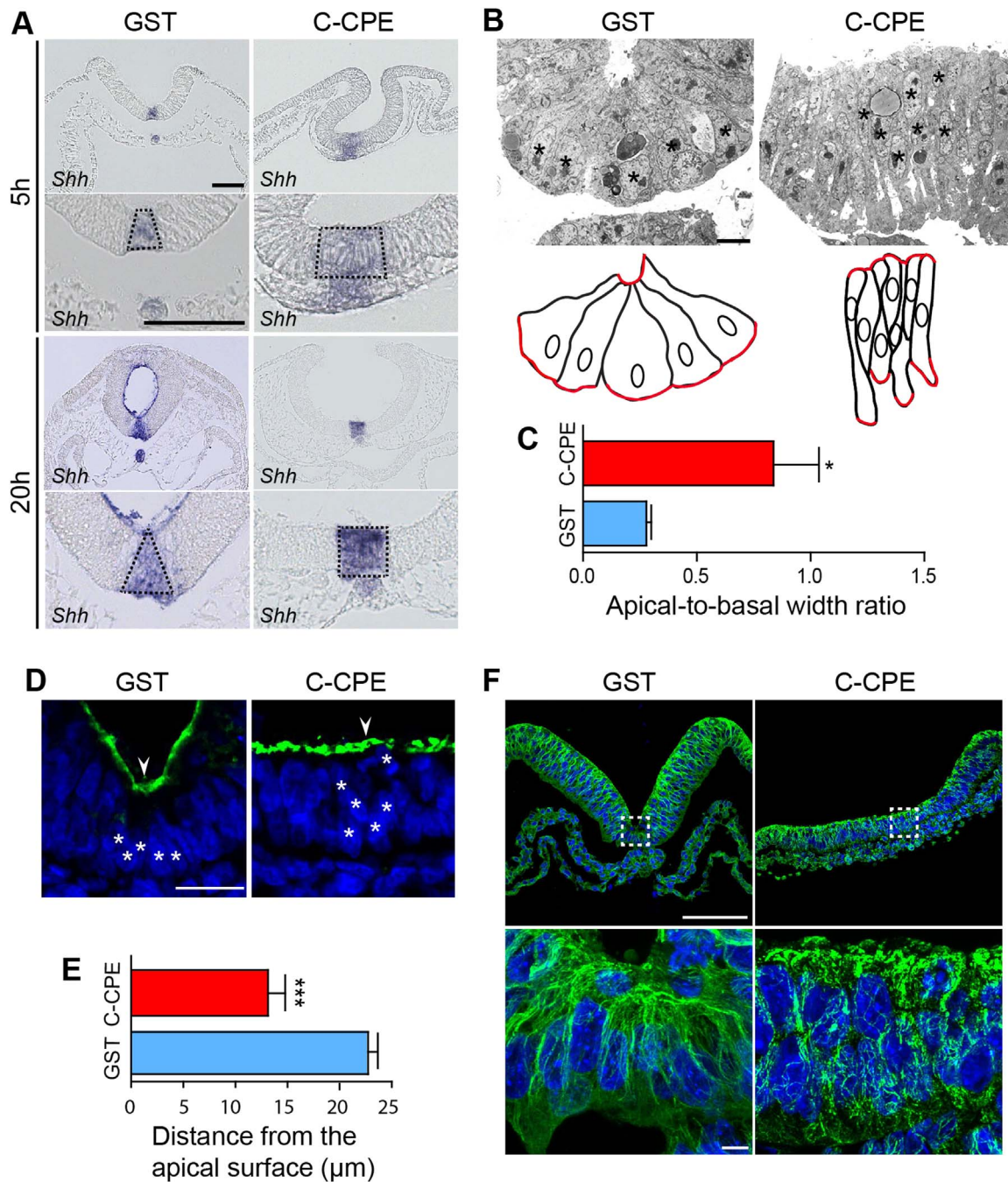


Fig. 5. Neural plate midline cells are not apically constricted in C-CPE-treated embryos. **(A)** Transverse sections showing *Shh* expression in 5 h and 20 h GST- and C-CPE-treated embryos. Dashed line in higher magnification view marks *Shh* expression domain in floor plate. Scale bar, 50 μm . **(B)** Ultrathin sections through the neural tube of 20 h GST- and C-CPE-treated embryos processed for TEM. Nuclei are indicated by asterisks. Schematic representation is shown below. Apical and basal cell surfaces are outlined in red. **(C)** Graph illustrates apical-to-basal width ratio of median hinge point cells from embryos treated with GST ($n=8$ cells/2 embryos) or C-CPE ($n=10$ cells/2 embryos) (mean \pm s.e.m, * $p=0.012$, student *t*-test). Scale bar, 5 μm . **(D)** Transverse sections of 5 h GST- or C-CPE-treated embryos stained for Cldn1 (green) and DAPI (blue). Midline (white arrowhead) and nuclei (asterisks) are indicated. Scale bar, 10 μm . **(E)** Graph shows average distance of nuclei from apical cell surface in GST- ($n=108$ cells/2 embryos) and C-CPE-treated embryos ($n=212$ cells/3 embryos) (mean \pm s.e.m, *** $p=0.0005$, student *t*-test). **(F)** Top, transverse sections of 5 h GST- or C-CPE-treated embryos stained for α -tubulin (green) and DAPI (blue). Bottom, high magnification view of microtubules in the median hinge point of GST- and C-CPE-treated embryos. Scale bar, 100 μm .

embryos and its localization was unchanged in C-CPE^{YL}-treated embryos (Fig. 6B, Supplementary Fig. 6A). However, after 5 h of C-CPE-treatment, we observed the loss of RhoA from tight junctions and a significant reduction in phosphorylated myosin light chain (pMLC) in the neural ectoderm of C-CPE-treated embryos (Fig. 6B,C). Quantitative analysis revealed that although the total amount of RhoA did not change ($p=0.7882$), the correlation between RhoA and ZO-1 in C-CPE-treated embryos was $\sim 40\%$ that of GST-treated embryos ($p=0.0052$). Both the total level of pMLC ($p=0.0023$) and its

distribution to tight junctions ($p < 0.0001$) were significantly reduced in C-CPE-treated embryos. Incubating embryos with the ROCK inhibitors GSK 269962 and Y-27632 did not affect the expression or localization of Cldn3, -4 or -8 (Supplementary Fig. 7), although they did reduce the level of pMLC and cause NTDs as previously reported (Fig. 6C) (Kinoshita et al., 2008; Escuin et al., 2015). These data further support that claudins function upstream of PCP and Rho/ROCK signaling during neural tube closure.

Analysis of apical-basal polarity suggested that the decreased apical

localization of Vangl2, RhoA and pMLC in C-CPE-treated embryos was not due to effects on the establishment or maintenance of apical-basal polarity. Cldn1, Cldn14, ZO-1 and 2, and F-actin were apically localized

in C-CPE-treated embryos (Figs. 1, 5D and 6). In both GST- and C-CPE-treated embryos Cldn1 was localized apical to the adherens junction protein E-cadherin (Fig. 7A), Par3 co-localized with ZO-1

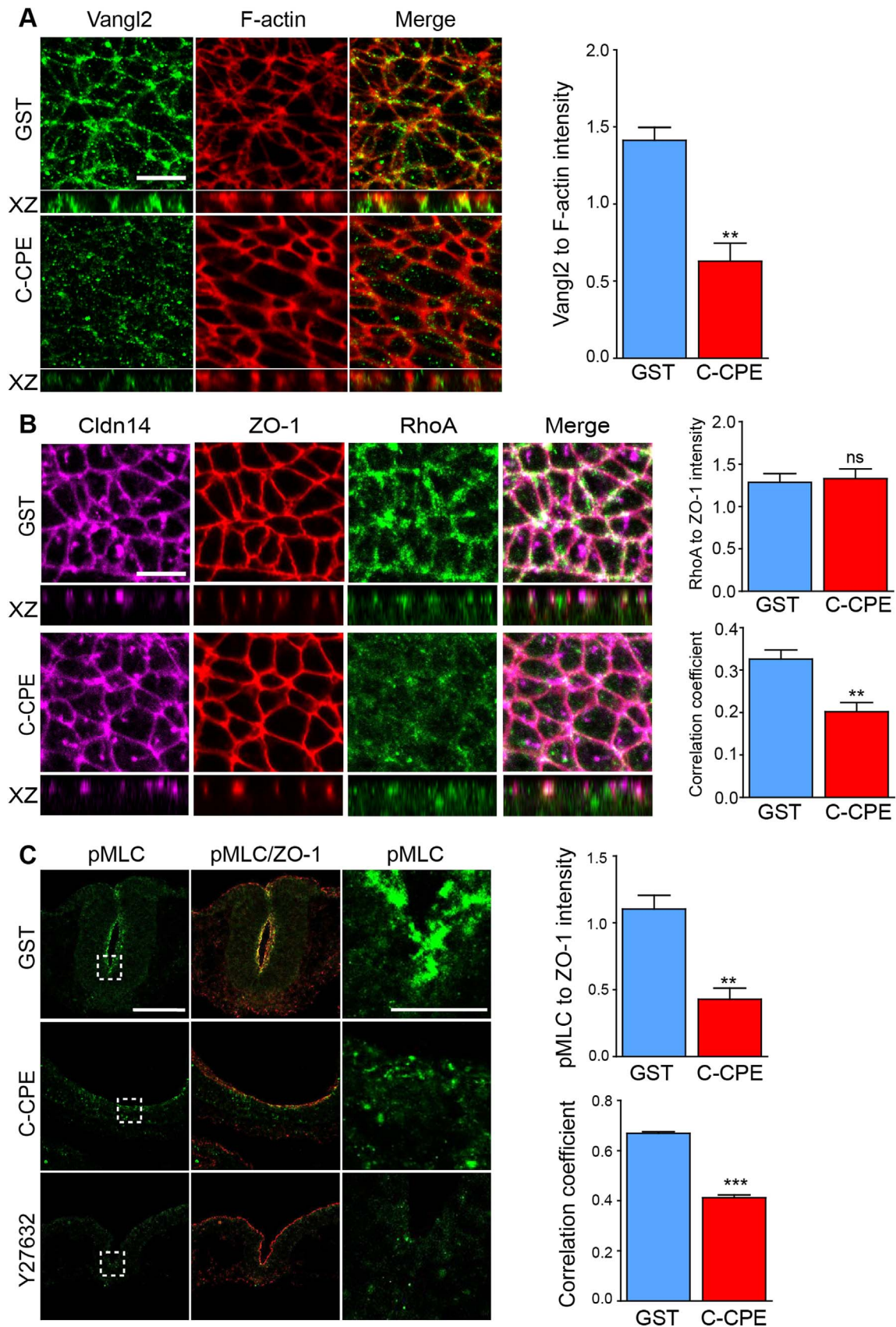


Fig. 6. PCP and RhoGTPase signaling proteins are reduced at tight junctions in C-CPE-treated embryos. **(A)** Apical surface and orthogonal (XZ) views of Vangl2 (green) and F-actin (Phalloidin, red) in neural ectoderm of GST- or C-CPE-treated embryos at 5 h. Scale bar, 10 μ m. Graph shows the ratio of the immunofluorescence intensity of Vangl2 to F-actin. Histogram represents an average of three embryos and values were calculated from maximum intensity projections (mean \pm s.e.m, **p=0.0024, student *t*-test). **(B)** Apical surface and orthogonal (XZ) views of Cldn14 (pink), ZO-1 (red), and RhoA (green) in the neural ectoderm of GST or C-CPE-treated embryos at 5 h. Scale bar, 10 μ m. Graphs show the ratio of the immunofluorescence intensity of RhoA to ZO-1 (upper), and Pearson's correlation coefficient for RhoA and ZO-1 (lower). Histograms represent an average of three different fields from three embryos and values were calculated from maximum intensity projections (mean \pm s.e.m, ns = not significant, **p=0.0052, student *t*-test). **(C)** Transverse sections of embryos treated with GST, C-CPE or Y27632 for 5 h showing pMLC (green) and ZO-1 (red). Scale bar, 100 μ m (left and middle) and 10 μ m (right). Graphs show the ratio of the immunofluorescence intensity of pMLC to ZO-1 (upper), and Pearson's correlation coefficient for pMLC and ZO-1 (lower). Data were collected from the enclosed areas of sectioned neural plates. Histograms represent an average of three embryos and values were calculated from maximum intensity projections (mean \pm s.e.m, **p=0.0023, ***p < 0.0001, student *t*-test).

(Fig. 7B) and ZO-2 localized apical to the Scribble complex protein Dlg1 (Fig. 7C). These data suggest that localization and/or retention of Vangl2, RhoA and pMLC to the apical membrane is dependent on the presence of C-CPE-sensitive claudins in the neural tube.

2.7. C-CPE treatment affects cell morphology and protein localization at the apical surface

Apical surface views showed that claudins, ZO scaffolding proteins, E-cadherin and F-actin localized normally to the lateral cell membranes in C-CPE-treated embryos (Figs. 2B and C, 6A and B and 7A). This was not the case for Par3; although restricted to the apical domain, large aggregates of Par3 were present in the cytoplasm (Fig. 7D). Similarly, the RhoGTPase Cdc42 was observed across the apical surface and less enriched at lateral membranes as compared to embryos treated with GST or C-CPE^{YL} (Fig. 7E, Supplementary Fig. 6B). Consistent with our visual analysis, we found that the total amount of Par3 (p=0.107) and Cdc42 (p=0.523) was not affected by C-CPE treatment, but that their distribution was altered (p < 0.05) (Fig. 7F). These data also support unique roles for individual claudins in maintaining protein complexes at the apical tight junction cytoplasmic plaque.

TEM analysis of tight junction ultrastructure revealed that electron dense tight junctions between cells at the neural plate midline in C-CPE-treated embryos were indistinguishable from those in GST-treated embryos (Fig. 7G). However, in C-CPE-treated embryos the apical surface of these cells was smooth, convex and devoid of microvilli (Fig. 7G) as compared to cells in GST-treated embryos, which contained numerous microvilli. Changes in morphology of the apical cell surface may be secondary to the altered localization of Cdc42, which is a critical regulator of the microtubule network. Together these data revealed roles for C-CPE-sensitive claudins in regulating the shape of the apical cell surface.

3. Discussion

Claudins are known to have distinct roles in determining cell shape (Wu et al., 2004; Nelson et al., 2010), maintaining epithelial integrity (Ikenouchi et al., 2003) and embryonic morphogenesis (Siddiqui et al., 2010). In this study, we demonstrated for the first time that claudins have a direct role in neural tube closure: C-CPE removal of Cldn3, -4 and -8 from tight junctions in the neural and non-neural ectoderm resulted in NTDs in chick and mouse embryos. Although disrupting ectoderm differentiation can affect neural tube closure (Kimura-Yoshida et al., 2015; Ybot-Gonzalez et al., 2007), gene expression analyses support that this is not the underlying cause of the C-CPE-induced NTDs. However, PCP and Par complex polarity proteins, and the small GTPases RhoA and Cdc42 were inappropriately localized at the apical cell surface in C-CPE-treated chick embryos. Consequently, convergent extension and apical constriction, two critical morphogenetic events that drive neural tube closure, were disrupted. Folic acid supplementation was unable to rescue the open NTDs in C-CPE-treated chick embryos suggesting that claudin-mediated morphogenetic events underlie at least a subset of NTDs not prevented by folic acid supplementation and fortification.

3.1. Claudins in convergent extension movements

Convergent extension, which coordinates anterior-posterior lengthening and mediolateral narrowing of the neural plate, is dependent on PCP signaling. C-CPE-treated embryos exhibited hallmarks of convergent extension defects similar to those observed in the PCP mouse mutants *Lp/Lp* and *Dvl1^{-/-};Dvl2^{-/-}* (Ybot-Gonzalez et al., 2007; Wang et al., 2006), suggesting that claudins and PCP signaling function in the same molecular pathway. The reduced expression of the core PCP protein Vangl2 in C-CPE-treated embryos positions claudins upstream of the PCP pathway in directing convergent extension cell movements. Furthermore, Vangl2 has been implicated in regulating anterior-posterior cell divisions during zebrafish neurulation (Ciruna et al., 2006) and we observed similar defects in oriented cell division in C-CPE-treated embryos. Therefore, we speculate that the loss of Vangl2 is responsible for the oriented cell division defects observed in these embryos. However, we cannot rule out the possibility that this is caused by disrupted localization of Par3 (Tawk et al., 2007) and Cdc42 (Kieserman and Wallingford, 2009) as they also play a role in oriented cell division. While a role for PCP-dependent convergent extension in avian neural tube closure has not been assessed, siRNA-mediated knockdown of the PCP component Celsr1 causes NTDs in chick embryos (Nishimura et al., 2012). This observation, along with the fact that overexpression and knockdown of PCP components causes convergent extension defects during neurulation in *Xenopus* (Goto and Keller, 2002; Wallingford and Harland, 2002) and zebrafish (Tawk et al., 2007) embryos, argues for a conserved role of the PCP pathway in regulating convergent extension during neural tube closure. Convergent extension defects were not observed in C-CPE-treated mouse embryos because C-CPE treatment was initiated at E8.5 after convergent extension is underway and neural tube closure has initiated. Interestingly, caudal elongation defects were observed in mouse embryos that were treated at the 0–4 somite stage (EN and NDEG, unpublished observations).

C-CPE removed claudins from the neural (Cldn4 and -8) and non-neural ectoderm (Cldn3 and -4), both of which undergo convergent extension movements. Decreased expression of *Cldn3*, -4, -6 and -7 in the non-neural ectoderm is also observed in *Grhl2* mutant mice, which have folate-resistant NTDs. Grainyhead-like 2 (*Grhl2*) is a transcription factor that is expressed exclusively in the non-neural ectoderm where it regulates expression of genes involved in epithelial identity, including claudins (Brouns et al., 2011; Pyrgaki et al., 2011; Werth et al., 2010). Although the neural folds remain widely spaced in the *Grhl2* mutants, convergent extension and apical constriction occur normally (Rifat et al., 2010; Pyrgaki et al., 2011; Werth et al., 2010). These data support our hypothesis that the convergent extension and apical constriction defects observed in C-CPE-treated embryos are due to the depletion of C-CPE-sensitive claudins from the neural ectoderm.

3.2. Claudins function upstream of RhoGTPase signaling during neural tube closure

Morphological, molecular and ultrastructure analysis of C-CPE-treated embryos revealed cells in the neural plate midline were not

apically constricted and consequently the median hinge point did not form. Establishment of the apical membrane domain in epithelial cells depends on the coordination of the intracellular trafficking machinery,

RhoGTPase signaling and the Par3-Par6-aPKC polarity complex. Despite a clear demarcation of the apical and basolateral domains in C-CPE-treated embryos, Par3 was abnormally localized in large

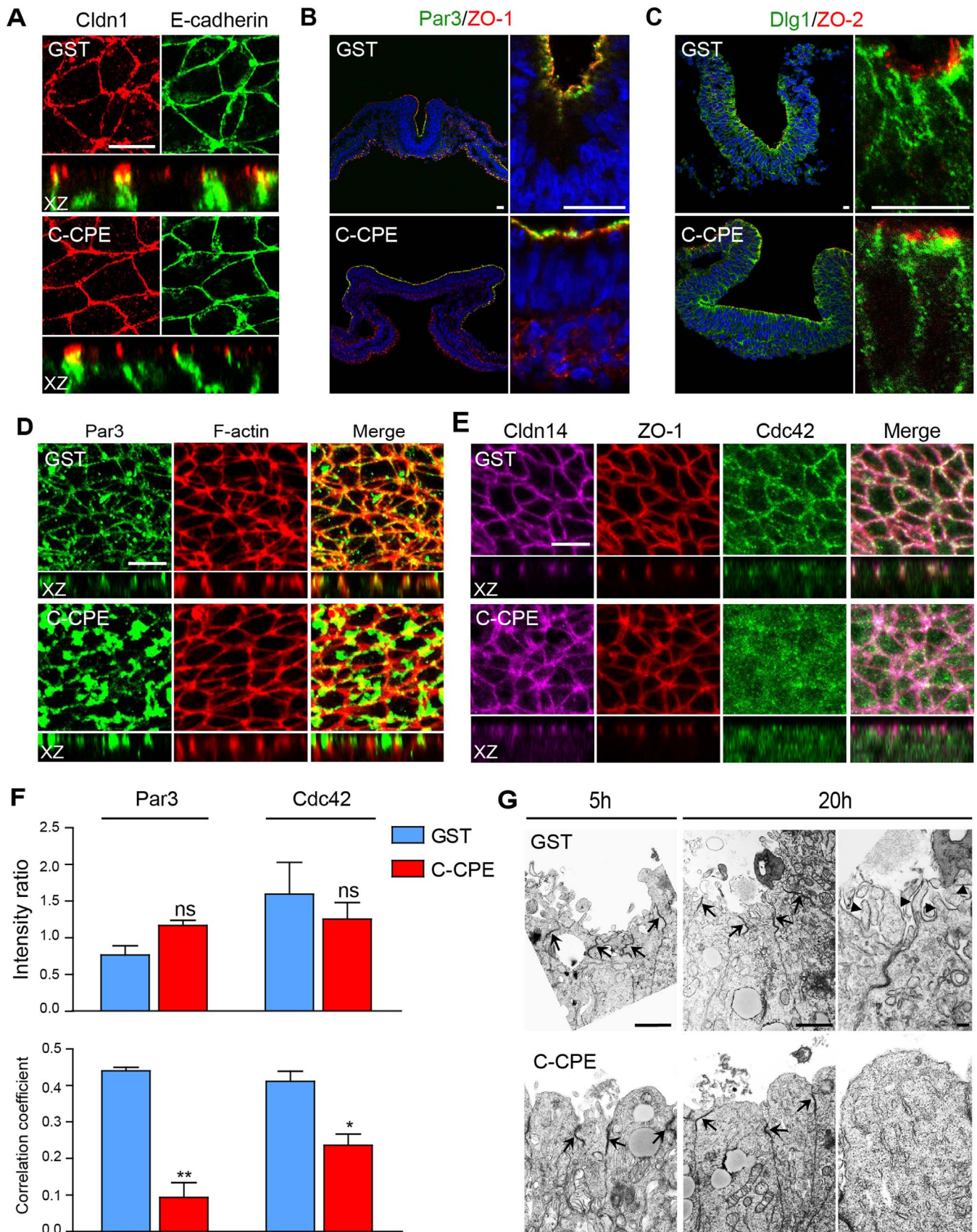


Fig. 7. C-CPE-sensitive claudins are required for Par3 and Cdc42 localization to the lateral membranes at the apical cell surface. (A) Apical surface and XZ orthogonal views of Cldn1 (red) and E-cadherin (green) in 5 h GST- and C-CPE-treated embryos. Scale bar, 20 μ m. (B) Transverse section from 5 h GST- and C-CPE-treated embryos showing Par3 (green) and ZO-1 (red). Scale bar, 20 μ m. (C) Transverse section from 5 h GST- and C-CPE-treated showing ZO-2 (red) and Dlg1 (green). Scale bar, 10 μ m. (D) Apical surface and XZ orthogonal views of Par3 (green) and F-actin (Phalloidin, red) in the neural ectoderm of 5 h GST- or C-CPE-treated embryos. Scale bar, 10 μ m. (E) Apical surface and XZ orthogonal views of Cldn14 (pink), ZO-1 (red) and Cdc42 (green) in the neural ectoderm of 5 h GST- or C-CPE-treated embryos. Scale bar, 10 μ m. Three embryos per treatment were analyzed. (F) Graphs show the ratio of the immunofluorescence intensity of Par3 to F-actin or Cdc42 to ZO-1 (upper), and Pearson's correlation coefficient for Par3 and F-actin or Cdc42 and ZO-1 (lower). Histograms represent an average of three different fields from three embryos and values were calculated from maximum intensity projections (mean \pm s.e.m, ns = not significant, * $p=0.0132$, ** $p=0.0072$, student *t*-test). (G) TEM micrographs of transverse sections at the neural tube midline of 5 h and 20 h GST- and C-CPE-treated embryos. Arrows indicate tight junctions and arrowheads indicate microvilli. Scale bar, 500 nm.

aggregates. Knockdown of Par3 in HH12 chick embryos, following neural tube closure, results in closed NTDs (Chen et al., 2017). Our data suggest that Par3 also plays a role during earlier stages of neurulation in avian embryos. We presume that the aggregated Par3 either cannot fulfill its normal function and/or interferes with other protein trafficking at the apical surface.

During neural tube closure, apical localization of RhoA-ROCK signaling components at the neural plate midline is required for phosphorylation of myosin light chain, which then moves along actin filaments to generate the contractile force required for apical constriction (Kinoshita et al., 2008; van Straaten et al., 2002). Chick embryos treated with C3, an inhibitor of Rho GTPases, develop NTDs (Kinoshita et al., 2008). Similarly, inhibiting Rho kinase (by Y27632) or myosin II motor activity (by blebbistatin) causes open NTDs in chick (Kinoshita et al., 2008) and mouse embryos (Escuin et al., 2015). In C-CPE-treated embryos, junctional localization of RhoA was reduced leading to reduced levels of pMLC. Treatment with ROCK inhibitors, which significantly decreased the level of pMLC and caused open NTDs (Kinoshita et al., 2008; Escuin et al., 2015), did not affect claudin expression or localization. These data indicate that claudins function upstream of RhoA-ROCK signaling in the neural ectoderm during neural tube closure and that recruitment and retention of RhoA at the cytoplasmic plaque is dependent on direct or indirect interactions with claudins expressed in the neural ectoderm.

RhoA signaling is required for changing the claudin composition of tight junctions via endocytosis (Quiros and Nusrat, 2014). In *Xenopus* embryos endocytosis acts downstream of actin-myosin contraction to remove excess membrane from the apical surface; inhibiting endocytosis leads to neural tube defects due to defective apical constriction (Lee and Harland, 2010). Currently there is no evidence to suggest that endocytosis is required for apical constriction of neural ectoderm cells in the chick embryo. However, it is tempting to speculate that RhoA interactions with Cldn8 and/or Cldn4 contribute to remodeling of the apical cell surface in the chick neural ectoderm via endocytosis.

Actin-myosin-dependent apical constriction in midline neural plate cells occurs in concert with apical-basal shortening and basal nuclear migration, which are dependent on an apically-basally aligned microtubule network. Nuclear migration was disrupted in C-CPE-treated embryos and Cdc42, a critical regulator of the microtubule network (Cadot et al., 2012; Palazzo et al., 2001), was expressed diffusely across the apical surface rather than being enriched at the lateral membrane. We hypothesize that the altered localization of Cdc42 affects microtubule-dependent events during median hinge point formation. Defects in the microtubule cytoskeleton may also underlie the altered shape of the apical surface of midline cells in C-CPE-treated embryos, which were smooth, convex and devoid of the microvilli present in control embryos. Our data indicate that Cldn8 and/or Cldn4, C-CPE-sensitive claudins expressed in the neural ectoderm, uniquely contribute to the retention of Par polarity complex proteins and Cdc42 at the lateral cell membrane at the neural plate midline.

In conclusion, we have defined new roles for C-CPE-sensitive claudins in regulating cell movements and shape changes that are critical for neural tube morphogenesis. Our data support a model where disturbing the claudin composition of tight junctions impacts protein complexes at the cytoplasmic plaque. Previous studies have

suggested that Vangl2 polarization and Rho-induced phosphorylation of myosin light chain participate in a mutually dependent feedback loop (Nishimura et al., 2012; Ossipova et al., 2015). Our data suggest that claudin function intersects with this pathway to regulate Vangl2 localization to the apical cell surface and phosphorylation of myosin light chain during convergent extension and apical constriction, respectively. Both of these events are intrinsic to the neural ectoderm, where Cldn4 and -8 are the only C-CPE-sensitive claudins, *Cldn4* null mice have closed neural tubes (Fujita et al., 2012) and *Cldn8* null mice have not yet been reported. In the mouse kidney, Cldn4 and -8 are known to interact and Cldn8 is required for recruitment of Cldn4 to the tight junction (Hou et al., 2010; Gong et al., 2015). Therefore, we hypothesize that Cldn8 collaborates with Cldn4 to participate in unique interactions with signaling complexes at the tight junction cytoplasmic plaque, which regulate the morphogenetic movements and cell shape changes required for neural plate elongation and median hinge point formation. Claudin C-terminal domains are highly variable between family members and are uniquely regulated by phosphorylation and other post-translational modifications, which can influence their interactions with proteins in the tight junction cytoplasmic plaque (Findley and Koval, 2009). While individual claudins may not be required to maintain the apical domain or tight junction integrity, they are likely to each have unique roles in regulating intracellular events that affect the actin cytoskeleton and cell behavior, potentially in a cell-type or tissue-specific manner. Future studies will be needed to understand how claudins anchor these proteins to the apical cell surface, to determine if these interactions are direct or indirect, and how they are influenced by post-translational modifications.

Few of the more than 200 NTD mouse models have led to the identification of genetic mutations associated with human NTDs (Harris and Juriloff, 2010; Kibar et al., 2007). This is likely due to the complex etiology of the disease which results from gene-environment and gene-gene interactions. While single claudin knock-out mice do not exhibit NTDs, we showed that simultaneous removal of Cldn3, -4 and -8 from tight junctions results in NTDs that parallel the phenotypically diverse NTDs that can result from a common underlying gene defect in humans (Juriloff and Harris, 2012; Lei et al., 2013; Robinson et al., 2012). There are numerous examples of diseases where birth defects result from mutations in multiple genes that act synergistically (Kim et al., 2016; Nanni et al., 1999; Kajiwaru et al., 1994; Katsanis et al., 2001). While there has been limited success in identifying mutations in the human orthologues of mouse candidate NTD genes, an approach that looks at multiple genes that interact in a signaling pathway may be more successful. Our discovery of roles for C-CPE-sensitive claudins in neural tube closure, and their intersection with pathways known to be involved in neural tube closure, including RhoGTPase and PCP signaling, suggests that the claudin family represents new candidates for NTDs in humans.

4. Materials and methods

4.1. Production of GST and GST-C-CPE fusion protein

Expression of GST, GST fused N-terminally to the C-terminal amino acids 185–319 (Moriwaki et al., 2007) and the variants C-

CPE^{LSID} (L254A/S256A/I258A/D284A) and C-CPE^{YL} (Y306A/L315A) cloned into pET14b or pGEX6P1 was induced by IPTG. GST fusion proteins were purified from *E. coli* BL21 as described previously (Protze et al., 2015; Veshnyakova et al., 2012) and dialyzed against PBS. Protein concentration was determined using the BCA Protein Kit (Thermo-Scientific, Rockford, USA) or Bio-Rad Protein Assay (BioRad, Mississauga, Canada).

4.2. Embryo culture

Fertilized eggs (Couvour Simetin, Mirabel, Canada) were incubated at 38.5 °C. Embryos were collected, staged according to Hamilton and Hamburger (HH) criteria (Hamburger and Hamilton, 1951) and cultured using the modified Cornish pasty method (Nagai et al., 2011). Purified GST or C-CPE (50–500 µg/ml), ROCK inhibitors Y27632 (50 µM; Abcam, Cambridge, UK) or GSK 269962 (1 µM; Axon Medchem, Reston, USA), and folic acid (100 µM or 1 mM) were added directly to the Cornish pasty culture medium to achieve the final concentrations indicated.

E8.5 mouse embryos (E0.5 is noon on the day after overnight mating) were dissected in Dulbecco's Modified Eagle's Medium containing 10% fetal calf serum. The yolk sac and amnion were left intact for whole embryo culture (Cockroft, 1990; Pryor et al., 2012). GST or C-CPE were diluted with PBS. Fast Green (0.5% solution) was added to visualize injection. Microinjection was performed using a hand-held glass micropipette. Needle tips were positioned in the amniotic cavity by traversing the yolk sac and amnion and 1–2 µl were injected, as previously described (Abdul-Aziz et al., 2009). Following 18 h of culture, embryos were examined. Yolk sac circulation was used as an indicator of viability, somites were counted as a measure of developmental progression, and length of the posterior neuropore was measured using an eyepiece graticule.

4.3. Immunofluorescence staining

Immunostaining was performed on paraffin sections (for α -tubulin), cryosections or whole embryos fixed in 4% PFA or 10% trichloroacetic acid at 4 °C. Samples were incubated overnight at 4 °C with primary antibodies: Cldn1, -4 and -8 (Invitrogen, Carlsbad, USA, 1:25–1:50), Cldn3 (Abcam, Cambridge, UK, 1:50), Cldn14 (Sigma Aldrich, Oakville, Canada, 1:25), ZO-1 and ZO-2 (Invitrogen, 1:50, Carlsbad, USA), anti-disphospho-myosin light chain (Thr18/Ser19) (Cell Signaling, Ipswich, USA, 1:50), RhoA and Cdc42 (Santa Cruz, Santa Cruz, USA, 1:50), Par3 (Millipore, Etobicoke, Canada, 1:250), Dlg1 (US Biologicals, Salem, USA, 1:50), E-cadherin (BD Transduction, San Jose, USA, 1:100), α -tubulin (Abcam, Cambridge, UK, 1:100) or Vangl2 (gift from Dr. M Montcouquiol, 1:500). Alexa Fluor-conjugated secondary antibodies (1:500) were added for 1 h at RT. F-actin was detected using Alexa Fluor-conjugated Phalloidin (Molecular Probes, Eugene, USA). Sections and flat-mounted embryos were coverslipped with SlowFade Gold with DAPI (Molecular Probes, Eugene, USA) and imaged using a Zeiss LSM780 laser scanning confocal microscope. Colocalization and immunofluorescence quantification was performed using ZEN 2012 SP1 software (Carl Zeiss Microscopy, Germany).

4.4. Whole mount *in situ* hybridization

Antisense digoxigenin-labeled riboprobes for *Sox2*, *AP-2 α* , *Pax7* (Khudyakov and Bronner-Fraser, 2009), *Otx2* (Chapman et al., 2002; 2003), *Shh*, *Brachyury*, and *Pax6* were used as previously described (Collins and Ryan, 2011). Embryos were photographed using a Leica M125 dissecting microscope with Infinity Capture software v5.0.2 (Lumenera Corp.). Paraffin-embedded embryos were sectioned and photographed using a Zeiss Axiophot compound microscope and AxioCamMRc camera with Axiovision v4.7.1.0 software.

4.5. Transmission electron microscopy

Specimens were prepared at the Facility for Electron Microscopy Research, McGill University. Embryos were fixed with 2.5% glutaraldehyde, 0.1% calcium chloride and 4% sucrose in 0.1 M sodium cacodylate buffer overnight at 4 °C, post-fixed with 1% aqueous osmium and 1.5% potassium ferrocyanide in 0.1 M sodium cacodylate for 2 h at 4 °C, dehydrated with a graded series of acetone, and embedded in epon. 100 nm sections were cut using an UltraCutE ultramicrotome (Reichert-Jung) and stained with uranyl acetate and Reynold's lead. Images were acquired on an FEI Techai 12 120 kV transmission electron microscope equipped with an AMT xR80C 8 megapixel CCD camera.

4.6. Morphometric assessment of axial length, length-to-width ratios, apical constriction and oriented cell division

Dorsal images of embryos were photographed using a Leica M125 dissecting microscope with Infinity Capture software v5.0.2 (Lumenera Corp.) and imported into SPOT Advanced image capture software (SPOT Imaging Solutions). Width of the neural folds or neural tube at the level of the first somite and anterior-posterior length were measured. To assess apical constriction, individual cells of the median hinge point were examined in transverse ultrathin sections processed for transmission electron microscopy from embryos treated for 20 h with GST or C-CPE. Cell surfaces were measured using ImageJ software. Basal nuclear migration was determined by drawing a perpendicular line from the apical surface to the apical tip of each DAPI-positive nucleus in GST- and C-CPE-treated embryos at 5 h. To quantify the orientation of cell division, z-stacks of embryos stained with DAPI were exported into ImageJ. A line was drawn between the mitotic spindles of anaphase cells and the angle between this axis and the midline of embryos was measured. The angles of divisions were then exported to Microsoft Excel and converted into a 0° to 90° range plot as previously described (Shafer et al., 2017). For statistical purposes, spindle orientation measurements were separated into three bins: 0–30° (rostral-caudal), 30–60° (diagonal) or 60–90° (medial-lateral).

4.7. Whole mount TUNEL assay

GST- or C-CPE-treated embryos (200 µg/ml) were fixed with 4% PFA overnight at 4 °C and assessed using the *in situ* cell death detection kit, AP (Roche, Montreal, Canada). Neural and non-neural ectoderm of each embryo was imaged at the level of the hindbrain and first and last somites. Cell death index was calculated by dividing the number of TUNEL-positive nuclei by the total number of cells, as determined by Phalloidin staining in each 125 µm by 125 µm region.

4.8. Statistical analyses

Statistical significance was evaluated using the Mann-Whitney *U*-test, student *t*-test or Wilcoxon's signed-rank test through GraphPad InStat software or SigmaStat v.2 (SPSS Inc).

Competing interests

The authors have no competing interests.

Acknowledgements

We thank Drs. K. Christensen C. Goodyer, I. Gupta, L. Hermo, L. Jerome-Majewska, L. McCaffrey, R. Rozen, P. Siegel and Y. Yamanaka for helpful discussions, M. Furuse for GST-C-CPE construct, M. Bronner for Pax7, S. Chapman for Otx2, and J. Mui (McGill University FEMR), M. Fu (RI-MUHC Imaging Platform) and D. Savery (UCL) for technical assistance. The authors acknowledge the

facilities and the scientific and technical assistance of the Facility for Electron Microscopy Research, McGill University.

AIB is the recipient of a doctoral studentship from Fonds de recherche du Québec – Santé (FRQS) (29939). This work was supported by the UK Medical Research Council (NDEG) (G0802163), the Deutsche Forschungsgemeinschaft (Grant number 1273/3-2 to DFG, KR and grant number PI 837/2-1 to GK, JP), the Natural Sciences and Engineering Research Council of Canada (234319) (AKR), and Canadian Institutes of Health Research (MOP-84583) (AKR). AKR is a member of the RI-MUHC, which is supported in part by the FRQS.

Appendix A. Supporting information

Supplementary data associated with this article can be found in the online version at <http://dx.doi.org/10.1016/j.ydbio.2017.05.013>.

References

- Anderson, W.J., Zhou, Q., Alcalde, V., Kaneko, O.F., Blank, L.J., Sherwood, R.I., Guseh, J.S., Rajagopal, J., Melton, D.A., 2006. Genetic targeting of the endoderm with claudin-6CreER. *Dev. Dyn.: Off. Publ. Am. Assoc. Anat.* **237** (2), 504–512.
- Ben-Yosef, T., Belyantseva, I.A., Saunders, T.L., Hughes, E.D., Kawamoto, K., Van Itallie, C.M., Beyer, L.A., Halsey, K., Gardner, D.J., Wilcox, E.R., et al., 2003. Claudin 14 knockout mice, a model for autosomal recessive deafness DFNB29, are deaf due to cochlear hair cell degeneration. *Hum. Mol. Genet.* **12** (16), 2049–2061.
- Brouns, M.R., et al., De Castro, S.C., Terwindt-Rouwenhorst, E.A., Massa, V., Hekking, J.W., Hirst, C.S., Savery, D., Muntz, C., Partridge, D., Lamers, W., 2011. Over-expression of Grhl2 causes spina bifida in the Axial defects mutant mouse. *Hum. Mol. Genet.* **20** (8), 1536–1546.
- Cadot, B., Gache, V., Vasyutina, E., Falcone, S., Birchmeier, C., Gomes, E.R., 2012. Nuclear movement during myotube formation is microtubule and dynein dependent and is regulated by Cdc42, Par6 and Par3. *EMBO Rep* **13** (8), 741–749.
- Chapman, S.C., Schubert, F.R., Schoenwolf, G.C., Lumsden, A., 2002. Analysis of spatial and temporal gene expression patterns in blastula and gastrula stage chick embryos. *Dev. Biol.* **245** (1), 187–199.
- Chapman, S.C., Schubert, F.R., Schoenwolf, G.C., Lumsden, A., 2003. Anterior identity is established in chick epiblast by hypoblast and anterior definitive endoderm. *Development (Cambridge, England)* **130** (21), 5091–5101.
- Chen, X., An, Y., Gao, Y., Guo, L., Rui, L., Xie, H., Sun, M., Lam Hung, S., Sheng, X., Zou, J., et al., 2017. Rare deleterious PARD3 variants in the aPKC-binding region are implicated in the pathogenesis of human cranial neural tube defects via disrupting apical tight junction formation. *Hum. Mutat* **38** (4), 378–389.
- Ciruna, B., Jenny, A., Lee, D., Mlodzik, M., Schier, A.F., 2006. Planar cell polarity signalling couples cell division and morphogenesis during neurulation. *Nature* **439** (7073), 220–224.
- Cockroft, D.L., 1990. Dissection and culture of postimplantation embryos. In: Copp, A.J., Cockroft, D.L. (Eds.), *Postimplantation Mammalian Embryos: A Practical Approach*. IRL Press, Oxford, 15–40.
- Colas, J.F., Schoenwolf, G.C., 2001. Towards a cellular and molecular understanding of neurulation. *Dev. Dyn.* **221** (2), 117–145.
- Colas, J.F., Schoenwolf, G.C., 2003. Assessing the contributions of gene products to the form-shaping events of neurulation: a transgenic approach in chick. *Genesis* **37** (2), 64–75.
- Collins, M.M., Ryan, A.K., 2011. Manipulating claudin expression in avian embryos. *Methods Mol. Biol.* **762**, 195–212.
- Collins, M.M., Baumholtz, A.I., Simard, A., Gregory, M., Cyr, D.G., Ryan, A.K., 2015. Claudin-10 is required for relay of left-right patterning cues from Hensen's node to the lateral plate mesoderm. *Dev. Biol.* **401** (2), 236–248.
- Collins, M.M., Baumholtz, A.I., Ryan, A.K., 2013. Claudin family members exhibit unique temporal and spatial expression boundaries in the chick embryo. *Tissue Barriers* **1**, e24517-24511-e24517-24514.
- Daugherty, B.L., Ward, C., Smith, T., Ritzenhaler, J.D., Koval, M., 2007. Regulation of heterotypic claudin compatibility. *J. Biol. Chem.* **282** (41), 30005–30013.
- Escuin, S., Vernay, B., Savery, D., Gurniak, C.B., Witke, W., Greene, N.D., Copp, A.J., 2015. Rho-kinase-dependent actin turnover and actomyosin disassembly are necessary for mouse spinal neural tube closure. *J. Cell Sci.* **128** (14), 2468–2481.
- Findley, M.K., Koval, M., 2009. Regulation and roles for claudin-family tight junction proteins. *IUBMB Life* **61** (4), 431–437.
- Fujita, H., Hamazaki, Y., Noda, Y., Oshima, M., Minato, N., 2012. Claudin-4 deficiency results in urothelial hyperplasia and lethal hydronephrosis. *PLoS One* **7** (12), e52272.
- Furuse, M., Hata, M., Furuse, K., Yoshida, Y., Haratake, A., Sugitani, Y., Noda, T., Kubo, A., Tsukita, S., 2002. Claudin-based tight junctions are crucial for the mammalian epidermal barrier: a lesson from claudin-1-deficient mice. *J. Cell Biol.* **156** (6), 1099–1111.
- Gong, Y., Wang, J., Yang, J., Gonzales, E., Perez, R., Hou, J., 2015. KLHL3 regulates paracellular chloride transport in the kidney by ubiquitination of claudin-8. *Proc. Natl. Acad. Sci. USA* **112** (14), 4340–4345.
- Goto, T., Keller, R., 2002. The planar cell polarity gene strabismus regulates convergence and extension and neural fold closure in *Xenopus*. *Dev. Biol.* **247** (1), 165–181.
- Gow, A., Southwood, C.M., Li, J.S., Pariali, M., Riordan, G.P., Brodie, S.E., Danias, J., Bronstein, J.M., Kachar, B., Lazzarini, R.A., 1999. CNS myelin and sertoli cell tight junction strands are absent in *Osp/claudin-11* null mice. *Cell* **99** (6), 649–659.
- Guney, O., Canbilgen, A., Williams, A.W., Konak, A., Acar, O., 2003. The effects of folic acid in the prevention of neural tube development defects caused by phenytoin in early chick embryos. *Spine* **28**, 442–445.
- Gunzel, D., Yu, A.S., 2013. Claudins and the modulation of tight junction permeability. *Physiol. Rev.* **93**, 525–569.
- Hamburger, V., Hamilton, H.L., 1951. A series of normal stages in the development of the chick embryo. *J. Morphol.* **88** (1), 49–92.
- Harris, M.J., Juriloff, D.M., 2010. An update to the list of mouse mutants with neural tube closure defects and advances toward a complete genetic perspective of neural tube closure. *Birth Defects Res. A Clin. Mol. Teratol.* **88** (8), 653–659.
- Hou, J., Renigunta, A., Yang, J., Waldegger, S., 2010. Claudin-4 forms paracellular chloride channel in the kidney and requires claudin-8 for tight junction localization. *Proc. Nat. Acad. Sci. United States Am.* **107** (42), 18010–18015.
- Ikenouchi, J., Matsuda, M., Furuse, M., Tsukita, S., 2003. Regulation of tight junctions during the epithelium-mesenchyme transition: direct repression of the gene expression of claudins/occludin by Snail. *J. Cell Sci.* **116** (10), 1959–1967.
- Juriloff, D.M., Harris, M.J., 2012. A consideration of the evidence that genetic defects in planar cell polarity contribute to the etiology of human neural tube defects. *Birth defects research. Part A. Clin. Mol. Teratol.* **94**, 824–840.
- Kage, H., Flodby, P., Gao, D., Kim, Y.H., Marconett, C.N., DeMaio, L., Kim, K.J., Crandall, E.D., Borok, Z., 2014. Claudin 4 knockout mice: normal physiological phenotype with increased susceptibility to lung injury. *Am. J. Physiol. Lung Cell. Mol. Physiol.* **307** (7), L524–L536.
- Kajiwara, K., Berson, E.L., Dryja, T.P., 1994. Digenic retinitis pigmentosa due to mutations at the unlinked peripherin/RDS and ROM1 loci. *Science (New York, NY)* **264** (5165), 1604–1608.
- Karfunkel, P., 1971. The role of microtubules and microfilaments in neurulation in *Xenopus*. *Dev. Biol.* **25** (1), 30–56.
- Karfunkel, P., 1972. The activity of microtubules and microfilaments in neurulation in the chick. *J. Exp. Zool.* **181** (3), 289–301.
- Katahira, J., Inoue, N., Horiguchi, Y., Matsuda, M., Sugimoto, N., 1997. Molecular cloning and functional characterization of the receptor for Clostridium perfringens enterotoxin. *J. Cell Biol.* **136** (6), 1239–1247.
- Katahira, J., Sugiyama, H., Inoue, N., Horiguchi, Y., Matsuda, M., Sugimoto, N., 1997. Clostridium perfringens enterotoxin utilizes two structurally related membrane proteins as functional receptors in vivo. *J. Biol. Chem.* **272** (42), 26652–26658.
- Katsanis, N., Ansley, S.J., Badano, J.L., Eichers, E.R., Lewis, R.A., Hoskins, B.E., Scambler, P.J., Davidson, W.S., Beales, P.L., Lupski, J.R., 2001. Triallelic inheritance in Bardet-Biedl syndrome, a Mendelian recessive disorder. *Science (New York, NY)* **293** (5538), 2256–2259.
- Khudyakov, J., Bronner-Fraser, M., 2009. Comprehensive spatiotemporal analysis of early chick neural crest network genes. *Dev. Dyn.: Off. Publ. Am. Assoc. Anat.* **283** (3), 716–723.
- Kibar, Z., Capra, V., Gros, P., 2007. Toward understanding the genetic basis of neural tube defects. *Clin. Genet.* **71** (4), 295–310.
- Kibar, Z., Salem, S., Bosoi, C.M., Pauwels, E., De Marco, P., Merello, E., Bassuk, A.G., Capra, V., Gros, P., 2011. Contribution of VANGL2 mutations to isolated neural tube defects. *Clin. Genet.* **80** (1), 76–82.
- Kieserman, E.K., Wallingford, J.B., 2009. In vivo imaging reveals a role for Cdc42 in spindle positioning and planar orientation of cell divisions during vertebrate neural tube closure. *J. Cell Sci.* **122** (14), 2481–2490.
- Kim, E., Harris, A., Hyland, V., Murrell, D., 2016. Digenic Inheritance in Epidermolysis Bullosa Simplex involving two novel mutations in KRT5 and KRT14. *Br. J. Dermatol.*
- Kimura-Yoshida, C., Mochida, K., Ellwanger, K., Niehrs, C., Matsuo, T., 2015. Fate specification of neural plate border by canonical wnt signaling and Grhl3 is crucial for neural tube closure. *EBioMedicine* **2** (6), 513–527.
- Kinoshita, N., Sasai, N., Misaki, K., Yonemura, S., 2008. Apical accumulation of Rho in the neural plate is important for neural plate cell shape change and neural tube formation. *Mol. Biol. Cell* **19** (5), 2289–2299.
- Krause, G., Protze, J., Piontek, J., 2015. Assembly and function of claudins: Structure-function relationships based on homology models and crystal structures. *Semin. Cell Dev. Biol.* **42**, 3–12.
- Lawson, A., Anderson, H., Schoenwolf, G.C., 2001. Cellular mechanisms of neural fold formation and morphogenesis in the chick embryo. *Anat. Rec.* **262** (2), 153–168.
- Lee, J.Y., Harland, R.M., 2010. Endocytosis is required for efficient apical constriction during *Xenopus* gastrulation. *Current Biol. : CB* **20** (3), 253–258.
- Lei, Y., Zhu, H., Duhon, C., Yang, W., Ross, M.E., Shaw, G.M., Finnell, R.H., 2013. Mutations in planar cell polarity gene SCRIB are associated with spina bifida. *PLoS One* **8**, e69262.
- Li, G., Flodby, P., Luo, J., Kage, H., Sipos, A., Gao, D., Ji, Y., Beard, L.L., Marconett, C.N., DeMaio, L., et al., 2014. Knockout mice reveal key roles for claudin 18 in alveolar barrier properties and fluid homeostasis. *Am. J. Respir. Cell Mol. Biol.* **51** (2), 210–222.
- Lohrberg, D., Krause, E., Schumann, M., Piontek, J., Winkler, L., Blasig, I.E., Haseloff, R.F., 2009. A strategy for enrichment of claudins based on their affinity to Clostridium perfringens enterotoxin. *BMC Mol. Biol.* **10**, 61.
- Miyamoto, T., Morita, K., Takemoto, D., Takeuchi, K., Kitano, Y., Miyakawa, T., Nakayama, K., Okamura, Y., Sasaki, H., Miyachi, Y., et al., 2005. Tight junctions in Schwann cells of peripheral myelinated axons: a lesson from claudin-19-deficient mice. *J. Cell Biol.* **169** (3), 527–538.
- Morita, K., Sasaki, H., Furuse, M., Tsukita, S., 1999. Endothelial claudin: claudin-5/TMVCFC constitutes tight junction strands in endothelial cells. *J. Cell Biol.* **147** (1), 185–194.

- Moriwaki, K., Tsukita, S., Furuse, M., 2007. Tight junctions containing claudin 4 and 6 are essential for blastocyst formation in preimplantation mouse embryos. *Dev. Biol.* **312** (2), 509–522.
- Moury, J.D., Schoenwolf, G.C., 1995. Cooperative model of epithelial shaping and bending during avian neurulation: autonomous movements of the neural plate, autonomous movements of the epidermis, and interactions in the neural plate/epidermis transition zone. *Dev. Dyn.: Off. Publ. Am. Assoc. Anat.* **204** (3), 323–337.
- Murdoch, J.N., Doudney, K., Paternotte, C., Copp, A.J., Stanier, P., 2001. Severe neural tube defects in the loop-tail mouse result from mutation of *Lpp1*, a novel gene involved in floor plate specification. *Hum. Mol. Genet.* **10** (22), 2593–2601.
- Nagai, H., Lin, M.C., Sheng, G., 2011. A modified cornish pasty method for ex ovo culture of the chick embryo. *Genesis* **49** (1), 46–52, (New York, NY : 2000).
- Nanni, L., Ming, J.E., Bocian, M., Steinhaus, K., Bianchi, D.W., Die-Smulders, C., Giannotti, A., Imaizumi, K., Jones, K.L., Campo, M.D., et al., 1999. The mutational spectrum of the sonic hedgehog gene in holoprosencephaly: SHH mutations cause a significant proportion of autosomal dominant holoprosencephaly. *Hum. Mol. Genet.* **8** (13), 2479–2488.
- Nelson, K.S., Furuse, M., Beitel, G.J., 2010. The Drosophila Claudin Kune-kune is required for septate junction organization and tracheal tube size control. *Genetics* **185** (3), 831–839.
- Nishimura, T., Honda, H., Takeichi, M., 2012. Planar cell polarity links axes of spatial dynamics in neural-tube closure. *Cell* **149** (5), 1084–1097.
- Ossipova, O., Kim, K., Sokol, S.Y., 2015. Planar polarization of Vangl2 in the vertebrate neural plate is controlled by Wnt and Myosin II signaling. *Biol. Open* **4** (6), 722–730.
- Pai, Y.J., Abdullah, N.L., Mohd-Zin, S.W., Mohammed, R.S., Rolo, A., Greene, N.D., Abdul-Aziz, N.M., Copp, A.J., 2012. Epithelial fusion during neural tube morphogenesis. *Birth Defects Res. Part A, Clin. Mol. Teratol.* **94** (10), 817–823.
- Palazzo, A.F., Joseph, H.L., Chen, Y.J., Dujardin, D.L., Alberts, A.S., Pfister, K.K., Vallee, R.B., Gunderson, G.G., 2001. Cdc42, dynein, and dynactin regulate MTOC reorientation independent of Rho-regulated microtubule stabilization. *Curr. Biol.: CB* **11** (19), 1536–1541.
- Protze, J., Eichner, M., Piontek, A., Dinter, S., Rossa, J., Blecharz, K.G., Vajkoczy, P., Piontek, J., Krause, G., 2015. Directed structural modification of Clostridium perfringens enterotoxin to enhance binding to claudin-5. *Cell Mol. Life Sci.* **72** (7), 1417–1432.
- Pryor, S.E., Massa, V., Savery, D., Greene, N.D., Copp, A.J., 2012. Convergent extension analysis in mouse whole embryo culture. *Methods Mol. Biol.* **839**, 133–146.
- Pyrgaki, C., Liu, A., Niswander, L., 2011. Grainyhead-like 2 regulates neural tube closure and adhesion molecule expression during neural fold fusion. *Dev. Biol.* **353** (1), 38–49.
- Quiros, M., Nusrat, A., 2014. RhoGTPases, actomyosin signaling and regulation of the epithelial Apical Junctional Complex. *Semin. Cell Dev. Biol.* **36**, 194–203.
- Rifat, Y., Parekh, V., Wilanowski, T., Hislop, N.R., Auden, A., Ting, S.B., Cunningham, J.M., Jane, S.M., 2010. Regional neural tube closure defined by the Grainy head-like transcription factors. *Dev. Biol.* **345** (2), 237–245.
- Robinson, A., Escuin, S., Doudney, K., Vekemans, M., Stevenson, R.E., Greene, N.D., Copp, A.J., Stanier, P., 2012. Mutations in the planar cell polarity genes CELSR1 and SCRIB are associated with the severe neural tube defect craniorachischisis. *Hum. Mutat.* **33**, 440–447.
- Sausedo, R.A., Smith, J.L., Schoenwolf, G.C., 1997. Role of nonrandomly oriented cell division in shaping and bending of the neural plate. *J. Comp. Neurol.* **381** (4), 473–488.
- Shafer, M.E.R., Nguyen, A.H.T., Tremblay, M., Viala, S., Béland, M., Bertos, N.R., Park, M., Bouchard, M., 2017. Lineage Specification from Prostate Progenitor Cells Requires Gata3-Dependent Mitotic Spindle Orientation. *Stem Cell Reports* **8** (4), 1018–1031.
- Shrestha, A., McClane, B.A., 2013. Human claudin-8 and -14 are receptors capable of conveying the cytotoxic effects of Clostridium perfringens enterotoxin. *mBio* **4**, 1.
- Siddiqui, M., Sheikh, H., Tran, C., Bruce, A.E., 2010. The tight junction component Claudin E is required for zebrafish epiboly. *Dev. Dyn.: Off. Publ. Am. Assoc. Anat.* **239** (2), 715–722.
- Smith, J.L., Schoenwolf, G.C., 1987. Cell cycle and neuroepithelial cell shape during bending of the chick neural plate. *Anat. Rec.* **218** (2), 196–206.
- Sonoda, N., Furuse, M., Sasaki, H., Yonemura, S., Katahira, J., Horiguchi, Y., Tsukita, S., 1999. Clostridium perfringens enterotoxin fragment removes specific claudins from tight junction strands: Evidence for direct involvement of claudins in tight junction barrier. *J. Cell Biol.* **147** (1), 195–204.
- Suzuki, M., Morita, H., Ueno, N., 2012. Molecular mechanisms of cell shape changes that contribute to vertebrate neural tube closure. *Dev. Growth Differ.* **54**, 266–276.
- Suzuki, H., Tani, K., Tamura, A., Tsukita, S., Fujiyoshi, Y., 2015. Model for the architecture of claudin-based paracellular ion channels through tight junctions. *J. Mol. Biol.* **427**, 291–297.
- Tamura, A., Kitano, Y., Hata, M., Katsuno, T., Moriwaki, K., Sasaki, H., Hayashi, H., Suzuki, Y., Noda, T., Furuse, M., et al., 2008. Megaintestine in claudin-15-deficient mice. *Gastroenterology* **134** (2), 523–534.
- Tawk, M., Araya, C., Lyons, D.A., Reugels, A.M., Girdler, G.C., Bayley, P.R., Hyde, D.R., Tada, M., Clarke, J.D., 2007. A mirror-symmetric cell division that orchestrates neuroepithelial morphogenesis. *Nature* **446** (7137), 797–800.
- van der Linden, I.J., Afman, L.A., Heil, S.G., Blom, H.J., 2006. Genetic variation in genes of folate metabolism and neural-tube defect risk. *Proc. Nutr. Soc.* **65**, 204–215.
- van Straaten, H.W., Sieben, I., Hekking, J.W., 2002. Multistep role for actin in initial closure of the mesencephalic neural groove in the chick embryo. *Dev. Dyn.: Off. Publ. Am. Assoc. Anat.* **224** (1), 103–108.
- Veshnyakova, A., Piontek, J., Protze, J., Waziri, N., Heise, I., Krause, G., 2012. Mechanism of Clostridium perfringens enterotoxin interaction with claudin-3/-4 protein suggests structural modifications of the toxin to target specific claudins. *J. Biol. Chem.* **287** (3), 1698–1708.
- Wallingford, J.B., Harland, R.M., 2002. Neural tube closure requires Dishevelled-dependent convergent extension of the midline. *Development (Cambridge, England)* **129** (24), 5815–5825.
- Wang, J., Hamblet, N.S., Mark, S., Dickinson, M.E., Brinkman, B.C., Segil, N., Fraser, S.E., Chen, P., Wallingford, J.B., Wynshaw-Boris, A., 2006. Dishevelled genes mediate a conserved mammalian PCP pathway to regulate convergent extension during neurulation. *Development (Cambridge, England)* **133** (9), 1767–1778.
- Weil, M., Abeles, R., Nachmany, A., Gold, V., Michael, E., 2004. Folic acid rescues nitric oxide-induced neural tube closure defects. *Cell Death Differ.* **11**, 361–363.
- Werth, M., Walentin, K., Aue, A., Schonheit, J., Wuebken, A., Pode-Shakked, N., Vilianovitch, L., Erdmann, B., Dekel, B., Bader, M., et al., 2010. The transcription factor grainyhead-like 2 regulates the molecular composition of the epithelial apical junctional complex. *Development (Cambridge, England)* **137** (22), 3835–3845.
- Winkler, L., Gehring, C., Wenzel, A., Muller, S.L., Piehl, C., Krause, G., Blasig, I.E., Piontek, J., 2009. Molecular determinants of the interaction between Clostridium perfringens enterotoxin fragments and claudin-3. *J. Biol. Chem.* **284** (28), 18863–18872.
- Wu, V.M., Schulte, J., Hirschi, A., Tepass, U., Beitel, G.J., 2004. Sinuous is a Drosophila claudin required for septate junction organization and epithelial tube size control. *J. Cell Biol.* **164** (2), 313–323.
- Ybot-Gonzalez, P., Savery, D., Gerrelli, D., Signore, M., Mitchell, C.E., Faux, C.H., Greene, N.D., Copp, A.J., 2007. Convergent extension, planar-cell-polarity signalling and initiation of mouse neural tube closure. *Development (Cambridge, England)* **134** (4), 789–799.